Atmospheric Humidity Deficits Tell Us How Soil Moisture Deficits Down-Regulate Ecosystem Evaporation

Dennis D. Baldocchi*, Nicole Keeney*, Camilo Rey-Sanchez*, Joshua B. Fisher#

*130 Mulford Hall
Department of Environmental Science, Policy and Management
University of California, Berkeley
Berkeley, CA USA 94520

Corresponding author: baldocchi@berkeley.edu

Joint Institute for Regional Earth System Science and Engineering
University of California, Los Angeles
Los Angeles, CA, 90095

March 4, 2022

Advances in Water Research, Revised, R2

Abstract

Knowing how actual evaporation is down-regulated from potential evaporation during periods with soil moisture deficits is one of the greatest challenges towards computing evaporation everywhere on a regular basis. We propose the hypothesis that vegetated landscapes transmit information on soil moisture deficits through its down-regulation of evaporation, which in turn affects the humidification and growth of the planetary boundary layer. To test this hypothesis, we examined how the evaporative fraction, defined as the ratio between actual and potential evaporation, corresponds with the soil moisture stress index, defined as the relative humidity with a power law dependence on vapor pressure deficit times a parameter, β.

We tested the parameterized soil moisture stress index with direct eddy covariance measurements of actual evaporation and computations of potential evaporation based on meteorological conditions, averaged on monthly time steps. The analysis was conducted on a dataset obtained from 144 FLUXNET sites. These sites spanned much of the world's climates and biomes and contained over 5900 months of observations.

Observations of the evaporative fraction fit the model of the soil moisture stress index best for semi-arid and arid ecosystems, and least for the humid and wet ecosystems. Consequently, a significant relationship between measurements of the evaporative fraction and soil moisture stress index held for about one-half of the population of sites. Under this condition, the median value of the parameter, β, was 1.41.

To investigate the mechanism of this empirical soil moisture stress index, we diagnosed it with a coupled evaporation-planetary boundary layer model. The soil moisture stress index is strongly related to surface resistance, as defined by inverting Penman-Monteith equation. Consequently, this index provides an independent estimate of surface resistance based on easy to measure mean monthly weather conditions like relative humidity and temperature. Thereby, this soil moisture stress index has potential to be applied to weather, climate and biogeochemical models and the interpretation of satellite derived evaporation products, like the one provided by the ECOSTRESS mission.

Key Words

FLUXNET, ECOSTRESS, Evaporation, Soil Moisture, Ecohydrology, Eddy Covariance, Biosphere-Atmosphere Interactions

Introduction

To address questions related to the water budget of the terrestrial biosphere, we need to assess evaporative fluxes everywhere and all the time (Jiang and Ryu, 2016; Jung et al., 2010; Miralles et al., 2011). Unfortunately, there is no one tool that does it all (Fisher et al., 2017; Seneviratne et al., 2010). Instead, a multiple constraints approach, using satellite remote sensing, networks of flux towers, land-atmosphere models and machine learning methods (Fisher et al., 2020; Jiang and Ryu, 2016; Jung et al., 2011), best meets this objective. However, there are conditions where and when the multiple constraints approach works best or fails.

What are these conditionalities and how can we best constrain this problem? For an extended, fully vegetated, landscape, with access to ample soil moisture, evaporation rates occur at a rate defined as potential evaporation (Budyko, 1974; Jarvis and McNaughton, 1986; Monteith, 1981; Priestley and Taylor, 1972). The flux density of potential evaporation (E_{pot}) can be approximated as 1.26 times the equilibrium evaporation (E_{eq}) rate (Priestley and Taylor, 1972). The rate of equilibrium evaporation is a function of available energy and temperature and is defined as:

$$E_{eq} = \frac{s}{s+\gamma}(R_n - G) \quad (1$$

In Eq 1, R_n is the net radiation balance, G is the heat conducted in and out of the soil, s is the slope of the saturation vapor pressure-temperature function, as defined by the Clausius Clapeyron equation (Wallace and Hobbs, 1977), and γ is the psychrometric constant. The exceedance of actual evaporation over equilibrium evaporation is achieved by feedbacks among heat and vapor fluxes at the land surface, the rate of growth of the boundary layer and the entrainment of dry, warm air from above the planetary boundary layer (McNaughton and Spriggs, 1986; Raupach, 2000).

Under ideal circumstances (well-watered vegetation with high leaf area indices), landscape and regional scale estimates of evaporation can be calculated with gridded information on net radiation (Anderson et al., 2019; Bastiaanssen et al., 1998; Jin et al., 2011). For this application, estimates of net radiation fields can be derived from sets of sensors on satellites that assess incoming solar radiation, albedo, emissivity, and surface temperature at a sensor-constrained pixel resolution (Anderson et al., 2007; Bastiaanssen et al., 1998; Hook et al., 1992; Jin et al., 2011; Mu et al., 2007; Verma et al., 2016). Soil heat storage, G, can be assumed to be nil when integrated over 24 hours or it can be computed as a function of net radiation when evaluated across landscape and regional space scales (Kustas and Daughtry, 1990; Purdy et al., 2016).

Many ecosystems are not well-watered or form fully vegetated, closed canopies. Hence, their actual evaporation rates occur at fractions of potential evaporation, as defined by the Priestley-Taylor rate (Budyko, 1974; Debruin, 1983; Jacobs and Debruin, 1992; Mallick et al., 2015; Mu et al., 2007; Seneviratne et al., 2010).

Knowing how actual evaporation is down-regulated from potential evaporation during periods with soil moisture deficits is one of the challenges towards computing evaporation everywhere on a regular basis. This down-regulation in potential evaporation is imposed most directly by reductions in surface conductance (Jarvis and McNaughton, 1986; McNaughton and Spriggs, 1986; Monteith, 1965; Raupach, 1995).

In practice, spatial and temporal variations in the surface conductance are difficult to estimate independently at landscape and regional scales. Surface conductance is a function of a diverse set of physical and physiological properties of the land. The most prominent governors of this conductance include the impacts of photosynthetic pathway and physiological capacity, leaf nitrogen, vapor pressure deficits and soil moisture on stomatal conductance and the impacts of water deficits and growth conditions on leaf area index (Baldocchi and Meyers, 1998; Kelliher et al., 1995; Kim and Verma, 1991; Novick et al., 2016; Stewart and Verma, 1992). On a spatial basis, across climate gradients and ecological space, the surface conductance is most sensitive to the vegetative fraction, or leaf area index of the landscape. In water limited ecosystems, the maximum leaf area index adjusts, to reach a

water balance between gains (precipitation) and losses (evaporation and runoff) (Grier and Running, 1977; Joffre and Rambal, 1993; Sankaran et al., 2005). In these water-limited cases, less vegetation leads to less transpiration, which provides another means for plants to transmit information on soil moisture deficits to the atmosphere.

Can there be another independent proxy of surface conductance that can be deduced from simpler and routine information, like weather conditions?; we ask this question knowing there is tight coupling between temperature, soil moisture, humidity deficits, precipitation and evaporation at regional and seasonal scales (Baldocchi, 1989; D'Odorico et al., 2007; Jarvis and McNaughton, 1986; Koster et al., 2004; Novick et al., 2016; Seneviratne et al., 2010; Wolf et al., 2016).

To answer this question, we propose an alternative approach--let vegetation serve as a sensor of plant-available, soil moisture. This information can be transmitted by the ability of an evaporating landscape to humidify the planetary boundary layer, which in turn reflects the state by which a down-regulation of actual evaporation may have occurred. The idea works as follows on a temporal basis. First, plants access soil moisture in the vadose zone by establishing a volume filling network of fibrous roots. As soil moisture declines, stomatal and hydraulic conductances and physiological capacity declines (Baldocchi, 1989; Schulze and Hall, 1982; Schulze et al., 1995; Sperry, 2000; Xu and Baldocchi, 2003). This decline imposes a reduction in plant transpiration which reduces latent heat exchange, increases sensible heat exchange, increases growth in the planetary boundary layer and decreases the humidification of the planetary boundary layer (McNaughton and Jarvis, 1991; Raupach, 1991; van Heerwaarden et al., 2009); or vice versa, it humidifies the boundary layer, enables convective clouds to form, which may rain and moisten the soil (Siqueira et al., 2009). The advantage of adopting this approach revolves around the fact that some plants develop deep roots which can tap ground water, a source of moisture that is not well detected by sensors in the soil (Baldocchi et al., 2021; Dawson et al., 2020; Miller et al., 2010; Rambal, 1984) or by satellite remote sensing, such as active and passive microwave radar (Entekhabi et al., 2010; Konings et al., 2019; Purdy et al., 2018).

Other support for the hypothesis that feedbacks between vegetation and the state of the planetary boundary layer can reflect the status of soil moisture is based on the successful use of simple evaporation models which simulated evaporation across climate and vegetation gradients in North America using relative humidity information (Fisher et al., 2008; Mu et al., 2011; Rigden and Salvucci, 2015; Salvucci and Gentine, 2013).

How will this approach, using plants to sense soil moisture, be achieved on a practical basis? We borrow and adapt an idea on how evaporation is being deduced by PT-JPL model which is being used to estimate evaporation for the ECOSTRESS mission (Fisher et al., 2020; Fisher et al., 2008). Since actual evaporation (E) is not equal to potential evaporation (E_{pot}) over vegetated landscapes suffering from soil moisture deficits, the PT-JPL evaporation retrieval imposes a set of ecophysiological constraint functions. One function down-regulates soil evaporation with an empirical soil moisture stress index (Fisher et al., 2020; Fisher et al., 2008; Mallick et al., 2013). This soil moisture stress index is defined as a function of relative humidity to the power of vapor pressure deficit (VPD, kPa), times a parameter β. The other function down-regulates transpiration as a fraction of observed to maximum fraction of absorbed sunlight.

Since the soil moisture constraint defines the relative extractable water (Fisher et al., 2008) and the plant transpiration constraint scales with relative extractable water (Chen et al., 2008; Feddes et al., 2001; Rodriguez-Iturbe, 2000), we propose the hypothesis that the soil moisture stress index, which varies between zero and one, can be used to down-regulate the evaporative fraction, defined as the ratio between actual and potential evaporation (which also ranges between zero and one) rather than only soil evaporation:

$$\frac{E}{E_{pot}} = RH^{\beta \cdot VPD} \quad (2$$

In Equation 2, RH is relative humidity, VPD is vapor pressure deficit and β is a free parameter.

Until now, the soil moisture stress index has not been evaluated across a spectrum of flux measurements sites that vary in climate, and ecosystem structure and function. In this paper we explore the utility and behavior of the soil moisture stress function using direct eddy covariance water vapor flux measurements from across the climate and ecological space of the global FLUXNET project (Pastorello et al., 2020). Then, we interpret its behavior and utility with a coupled surface layer-planetary boundary layer model (McNaughton and Spriggs, 1986).

Other reasons why we base this analysis on total evaporation, the sum of soil evaporation and plant transpiration, are because: 1) total evaporation affects the humidification and growth of the planetary boundary layer and 2) it is very difficult and uncertain to partition direct measurements of evaporation rates into its components, transpiration and soil evaporation, on a routine basis (Stoy et al., 2019).

Materials and Methods

Eddy Covariance Measurements of Evaporation, and Supporting Metadata

Continuous and long-term eddy covariance flux measurements of water vapor, sensible heat, CO_2 and momentum were made by independent teams of scientists, world-wide. Their data were submitted to a central data center, then vetted, harmonized, gap-filled and distributed through the auspices of the global network FLUXNET database (Papale et al., 2012; Pastorello et al., 2020).

Typical instrument systems for making eddy covariance flux measurements include 3-dimensional sonic anemometers and closed or open path infrared gas analyzers (Rebmann et al., 2018). Sensors were sampled 10 to 20 times per second. Flux covariances were computed for 30-minute time intervals using standard software that includes 3-dimensional, coordinate rotation and mean removal (Sabbatini et al., 2018). Simultaneous measurements were made of a set of driving meteorological and soil variables, too, such as solar radiation components, air temperature, wind speed and direction, soil moisture, soil temperature. The structural and functional attributes of each site were also characterized and are listed in the complementary Biological, Ancillary and Disturbance Metadata (BADM) database (https://fluxnet.org/badm-data-product/).

In this analysis we used monthly-averaged data from the FLUXNET 2015 CC by 4 dataset (https://fluxnet.org/data/fluxnet2015-dataset/). This analysis extracted data from 144 sites and contains over 5900 months of observation data; the chosen sites needed to pass our data quality criteria which included variables to compute potential evaporation. These measurement sites are distributed world-wide and cover a wide range of managed and natural landscapes from a variety of functional groups (crops, evergreen needleleaf and broadleaf forests, deciduous forests, savanna, grasslands, shrublands and wetlands). Details on the sites selected, their geographic location and digital objective identifier (DOI) of the datasets are listed in Supplementary Material.

We evaluated the beta parameter, β, in Equation 2 for each site using inputs from the multi-year time series of eddy covariance measurements of evaporation (E) and calculations of potential evaporation (E_{pot}). Potential evaporation was computed using the Priestley-Taylor equation (Priestley and Taylor, 1972), which is defined as 1.26 times equilibrium evaporation (Eq. 1). Inputs include independent measurements of net radiation (R_n), soil heat flux (G), and air temperature (T_a). To solve for β, we used corresponding measurements of vapor pressure deficit (VPD) and relative humidity (RH). We used the Broyden-Fletcher-Goldfarb-Shanno optimization (Broyden et al., 1973) to solve for a best fit β value in Python using the library scipy.optimize. Details of the Python code are presented in Supplemental Material.

Coupled Surface Energy Balance-Boundary Layer Growth Model

We computed the daily dynamics of surface energy fluxes and the atmospheric state variables, temperature and humidity mixing ratio in the mixed layer of the planetary boundary layer, by coupling an analytical solution to the surface energy balance (Paw U and Gao, 1988) to a one-dimensional, clear-sky planetary boundary layer model

(McNaughton and Spriggs, 1986). The model was evaluated recently against long term measurements of boundary layer growth (Rey-Sanchez et al., 2021).

We summarize the key attributes of the model, next. The model considers the exchange of heat and moisture in and out of the top and bottom of a column of air that is capped by the planetary boundary layer. The time rate of change of potential temperature (θ_m) in the mixed layer is a function of the height of the mixed layer, h, its time rate of change, dh/dt, sensible heat flux at the land surface (H) and the entrainment of warm air (θ_e) as the mixed layer grows and entrains air from the inversion above the mixed layer:

$$\rho C_p h \frac{d\theta_m}{dt} = H + \rho C_p (\theta_e - \theta_m) \frac{dh}{dt} \quad (3$$

The subscript m refers to the mixed layer and the subscript e refers to the air mass above the entrainment layer. Similarly, we can express the time rate of change of the mixing ratio of water vapor, q_m, in the mixed layer as:

$$\rho h \frac{dq_m}{dt} = E + \rho (q_e - q_m) \frac{dh}{dt} \quad (4$$

Here, the surface flux is defined by the evaporative flux density, E, ρ is air density and q_e is the mixing ratio of vapor above the entrainment layer. The additional unknown is the time rate of change of the height (h) of the planetary boundary mixed layer, dh/dt. The simplest scheme is:

$$\frac{dh}{dt} = \frac{H_v}{\rho C_p h \Gamma_v} \quad (5$$

In Equation 5, C_p is heat capacity at constant pressure and H_v is the virtual temperature heat flux, which is defined in terms of sensible (H) and latent heat flux (λE) densities:

$$H_v = (H + 0.07 \lambda E) \quad (6$$

Γ_v is the virtual temperature inversion strength. It is a function of the slopes of the inversions associated with potential temperature and specific humidity:

$$\Gamma_v = \Gamma_\theta + 0.61 \Gamma_q \quad (7$$

For sensitivity tests, the model was forced with temporal variations in sunlight representing a clear summer day; it varied between sunrise (0600 hours) and sunset (1800 hours) in a half-sinusoidal fashion with a midday peak of 1000 W m^{-2}. Initial conditions included an initial boundary layer height at 100 m, air temperature at 10 C, vapor pressure at 1 kPa, and albedo at 0.15. Simulations were conducted for a variety of values of surface and aerodynamic conductances and subsidence velocities to examine mechanistic response surfaces.

Results

The first question we address is how well the evaporative fraction and soil moisture stress index, described by Equation 2, correspond with one another as they vary with relative humidity. To answer this question and to provide a proof of concept, we start with a set of data from semi-arid savanna ecosystems; they were chosen because they experience the widest range of soil and atmospheric moisture content (Baldocchi et al., 2021; Cleverly et al., 2013; Meyer et al., 2015). Figure 1 shows that the lowest values of E/E_{pot} corresponded with the lowest values of RH, and vice versa. For perspective, we overlay calculated values of the soil moisture stress index based on the best fit β parameter for this functional type. The functional correspondence between the modeled values of the soil moisture stress index and measured values of the evaporative fraction were relatively good over this range of relative humidity, when assessed at monthly time scales (slope=1.12; R^2 = 0.74; RMSE = 0.1421). In other words, the soil moisture stress index captures the dynamics of the reduction in E/E_{pot} that occurs on a

seasonal basis over semi-arid ecosystems as soils and the atmosphere dry between the wet and dry seasons. On these longer (monthly) time steps, the humidity status of atmosphere and the supply of water transferred from the soil and through the plants were able to come to a degree of equilibrium, as opposed to variability and chaos associated with the passage of weather fronts that occur on daily to weekly time scales (Koster et al., 2004; Novick et al., 2016).

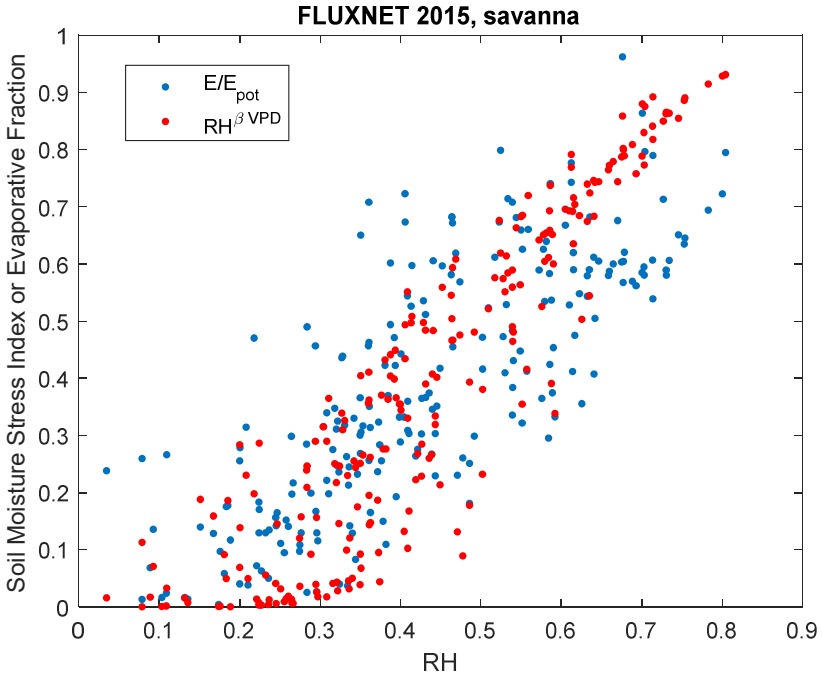

Figure 1 The dependency of soil moisture stress index or evaporative fraction on relative humidity (RH) for a set of seven (7) semi-arid savanna sites that experienced a wide range in soil moisture content. The blue colored dots are associated with computations of the soil moisture stress index as a function of relative humidity, air temperature and the optimized beta value (Table 1). The red dots are associated with measurements of E/E_{pot} at the corresponding FLUXNET sites.

The second question we address is how constant or variable the parameter, β, may be across the range of climate, and ecosystem function and structure that is represented across the FLUXNET network? Figure 2 shows a histogram of the β parameter that was determined for each of the FLUXNET sites used in this analysis. Computations of the beta parameter show a positively skewed distribution (skewness = 1.559) with a median of 1.710, a mean of 2.417 and a mode of 0.590. The upper tail of the histogram reaches 10 for a few sites.

For humid environments there may not be as wide a range in soil moisture stress index and relative humidity to provide robust statistical best fits. If we restrict the analysis for sites where slope of the best fit between the evaporative fraction and the soil moisture index is significantly different from zero ($p < 0.05$), then the population of sites used drops to 74 and the median, mean and mode shift to 1.41, 2.16, 0.59, respectively. In comparison, β was assumed to equal one in its first (Fisher et al., 2008) and current (Fisher et al., 2020) implementations for soil evaporation; this prior assumption split the two most populated bins of this histogram.

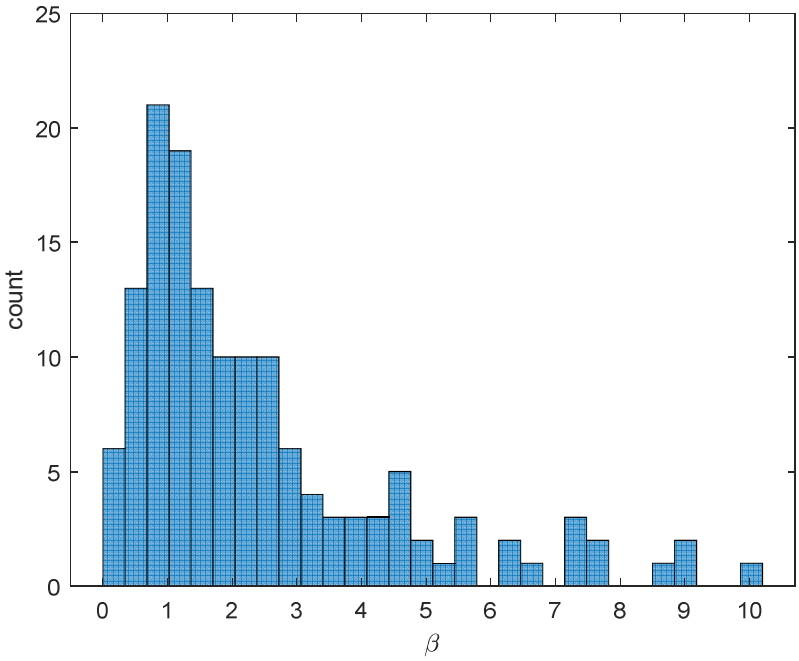

Figure 2 Histogram of the beta parameter, β, used to define the soil moisture constraint function. This histogram is based on beta values defined for each of the 144 sites used in the analysis.

To examine how well the fitted soil moisture constraint function performed with regards to direct evaporation measurements, we present a histogram that compares the difference between measured values of E/E_{pot} and computed values of $RH^{\beta\ VPD}$ for the many months recorded at each site (Figure 3). To remove unrepresentative biases from the winter dormant periods, these statistics were confined to conditions when the mean monthly air temperatures exceeded 5 C. The population mean difference was 0.0087, with 95% confidence intervals of +/- 0.0052. This difference was not significantly different from zero; p =0.0011; t = 3.256; df=4970. Hence, this model worked well enough across a large fraction of the population of FLUXNET data. On the other hand, there were locations where and when the simple soil moisture stress index model over- or underestimated measured values of evaporative fraction.

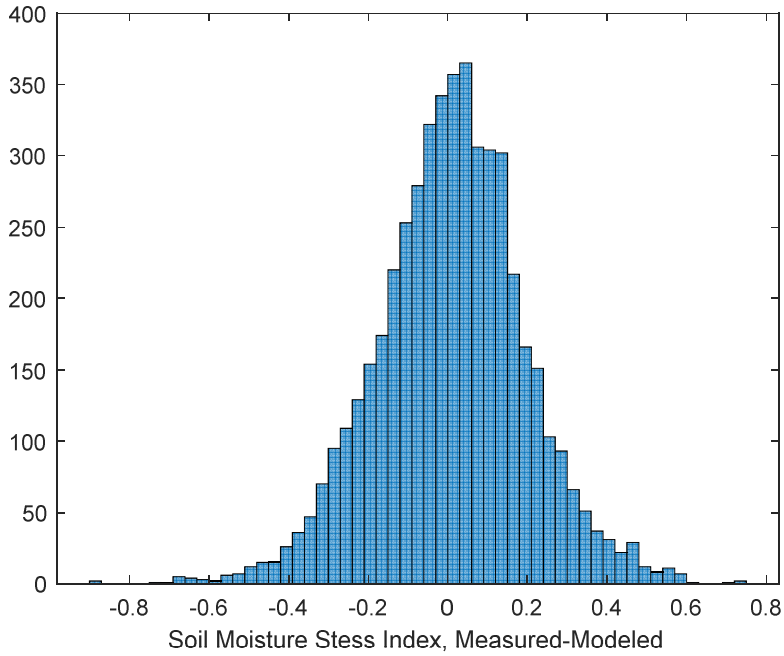

Figure 3 Histogram that reflects the difference between measured evaporative fraction (E/E_{pot}) and optimized soil moisture stress indices ($RH^{\beta_{VPD}}$) for 144 FLUXNET sites on a monthly basis.

Breaking up the data across broad functional groups we found that the performance of the soil moisture stress index fell into two categories (Table 1). One category experienced a strong statistical relation between evaporative fraction and the soil moisture stress index; slopes between the two variables ranged between 0.8 and 1.12 and their coefficient of determinations (R^2) exceeded 0.5. This group included semi-arid and arid sites, as associated with the closed and open shrublands, savanna, woody savanna, grasslands and evergreen broadleaved forests, like the eucalyptus in Australia, functional groups. Median values of β ranged between 0.59 and 4.3. Hence, there was no universal value for this group.

The other category experienced poor agreement between evaporative fraction and the soil moisture stress index. These functional groups experienced slopes between evaporative fraction and soil moisture index that were below 0.5 and possessed R^2 values below 0.2. This category was associated with the wetter and more humid sites (irrigated and rainfed crops, deciduous broadleaved forests, mixed and evergreen conifer forests and wetlands). We suspect that the soil moisture stress index performed most poorly for the humid ecosystems because they tended to experience a narrower range of climatological soil moisture deficits (see Supplemental Material). On the other hand, this method may work better over humid ecosystems when they experience modest to severe drought. However, a different value of β may emerge from such cases.

Table 1 Statistics on the beta, β, parameter for major International Geosphere Biosphere Program (IGBP) classes of vegetation. Also tabulated are the number of months used in the calculation and R^2, the slope between the dependent and independent variables and the coefficient of determination between the best fit parameter applied to the model (Equation 2) vs measurements of E/E_{pot}.

Functional Group	IGBP Class	β median	Number of months	slope	R^2
Closed Shrublands	CSH	4.325	78	0.852	0.757
Savannas	SAV	0.59	225	1.12	0.746
Woody Savannas	WSA	0.89	371	0.999	0.706
Grasslands	GRA	1.015	1036	0.871	0.657
Evergreen Broadleaf Forests	EBF	1.67	377	0.958	0.576
Open Shrublands	OSH	3.015	240	0.815	0.521
Croplands	CRO	1.25	692	0.392	0.177
Evergreen Needleleaf Forests	ENF	2.48	1646	0.417	0.126
Permanent Wetlands	WET	3.09	201	0.036	0.0721
Mixed Forests	MFX	2.705	399	0.281	0.0385
Deciduous Broadleaf Forests	DBF	1.79	680	0.192	0.025

Discussion

Both relative humidity and vapor pressure deficit are functions of the saturation vapor pressure, which is a function of absolute temperature (Wallace and Hobbs, 1977). Hence the soil moisture stress index is defined by a family of curves that are temperature dependent. The degree to which the soil moisture stress index is sensitive to temperature is shown in Figure 4. For a given relative humidity, the value of the soil moisture stress index increases as temperature decreases; for example, at a relative humidity of 0.6 the soil moisture stress index increases from about 0.5 to 0.85 as air temperature decreases from 30 to 10 C.

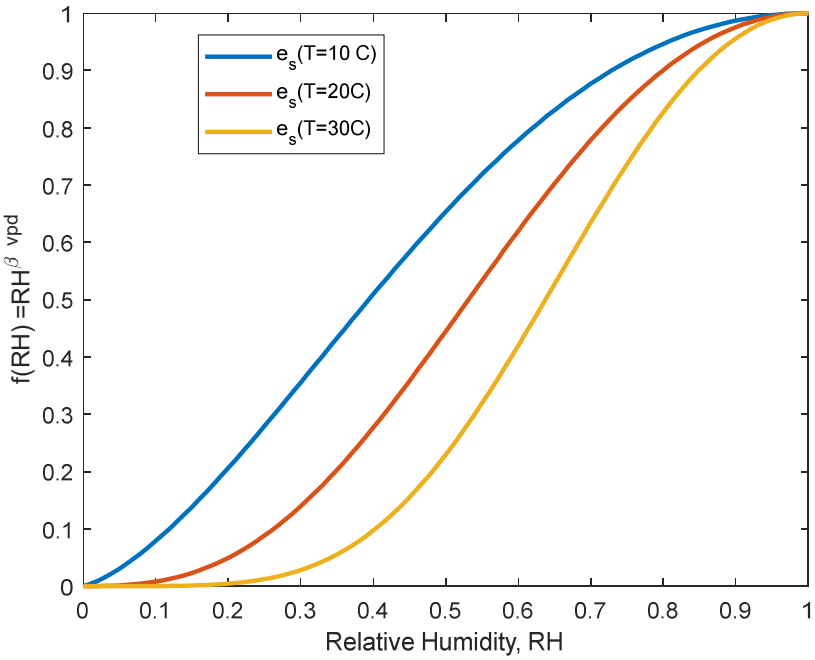

Figure 4 The sensitivity of the soil moisture stress index to air temperature, based on the corresponding value of saturation vapor pressure, e_s. β was assumed to equal one in these computations

The question begging to be asked is how and why this simple algorithm works relatively well to assess soil moisture deficits over vegetated landscapes? To answer this question, we diagnosed the Equation 2 by performing sensitivity calculations with the coupled E-PBL model. This was accomplished by performing simulations of diel patterns of temperature, specific humidity, sensible and latent heat exchange and planetary boundary layer growth for a set of surface and aerodynamic conductances for ideal summer growing conditions. These feedbacks between evaporation, atmospheric humidity and boundary layer growth yield a high-fidelity and corresponding response between the computation of the evaporative fraction, E/E_{pot}, computed values of the soil moisture stress index and variations in relative humidity (Figure 5).

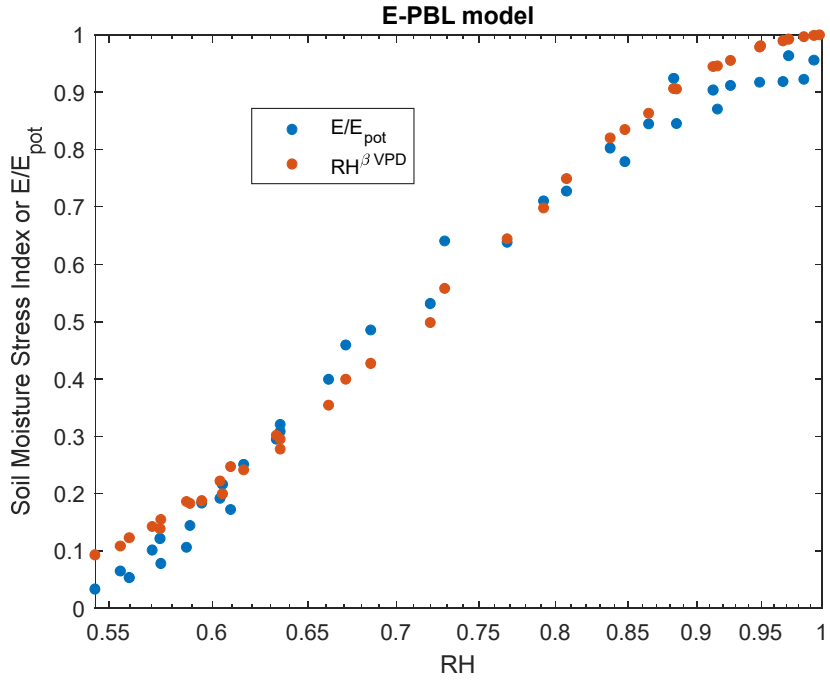

Figure 5 Comparisons of computations of evaporative fraction, as defined by the ratio between actual evaporation and potential evaporation and the soil moisture stress index, defined by Equation 2, as a function of relative humidity. The blue dots represent explicit calculations of E, E_{pot}, RH and VPD for a range of surface and aerodynamic resistances based on the E-PBL model. The red dots reflect the least square fit between computations of E/E_{pot} and RH and Equation 2. The optimal β for this case was 3.65. The computations assumed that subsidence velocity was zero.

To better understand why the soil moisture stress index works, we compared computations of the soil moisture stress index ($RH^{\beta\ vpd}$), derived from the E-PBL model with computations of the surface resistance (R_{sfc}), the inverse of surface conductance. Figure 6 shows a strong correspondence between the two metrics. In effect, this soil moisture stress index reflects how variations in a set of soil moisture related traits that are represented by surface resistance respond to changes in soil moisture and access to ground water and modulate the humidity of the atmospheric boundary layer; these traits include as leaf area index, stomatal conductance, soil evaporation and photosynthetic capacity (Baldocchi and Meyers, 1998). Hence, using this soil moisture stress index gives us an independent means to infer surface resistances using atmospheric humidity information

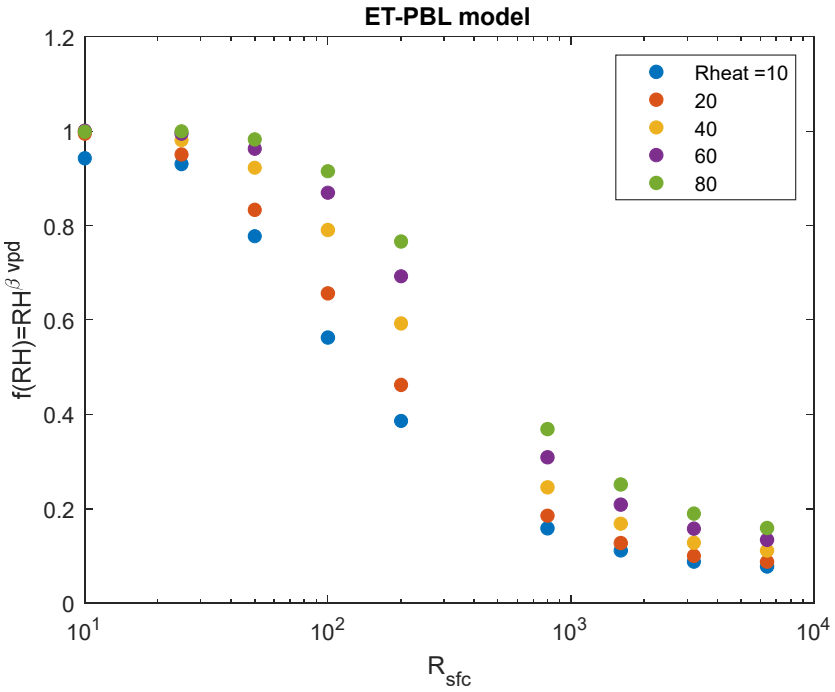

Figure 6 Variations in the soil moisture stress index to changes in surface resistance, R_{sfc} (s m^{-1}), the inverse of surface conductance. A family of curves for varying values of the boundary layer resistance for heat transfer (R_h) are shown. These computations were based on a coupled evaporation-planetary boundary layer, E-PBL, model.

Atmospheric subsidence velocity can affect the ultimate height of the planetary boundary layer on a given day (Molod et al., 2003; Myrup et al., 1983; Rey-Sanchez et al., 2021), which will affect the degree to which the boundary layer may or may not become humidified. For the set of computations, shown above, we assumed that the boundary layer subsidence velocity was zero. However, we find that there is a theoretical sensitivity of the β parameter to subsidence velocity. Subsidence velocities greater than zero lead to an increase in β and velocities less than zero lead to a decrease in β, which hits a plateau when β approaches 2 (Figure 7).

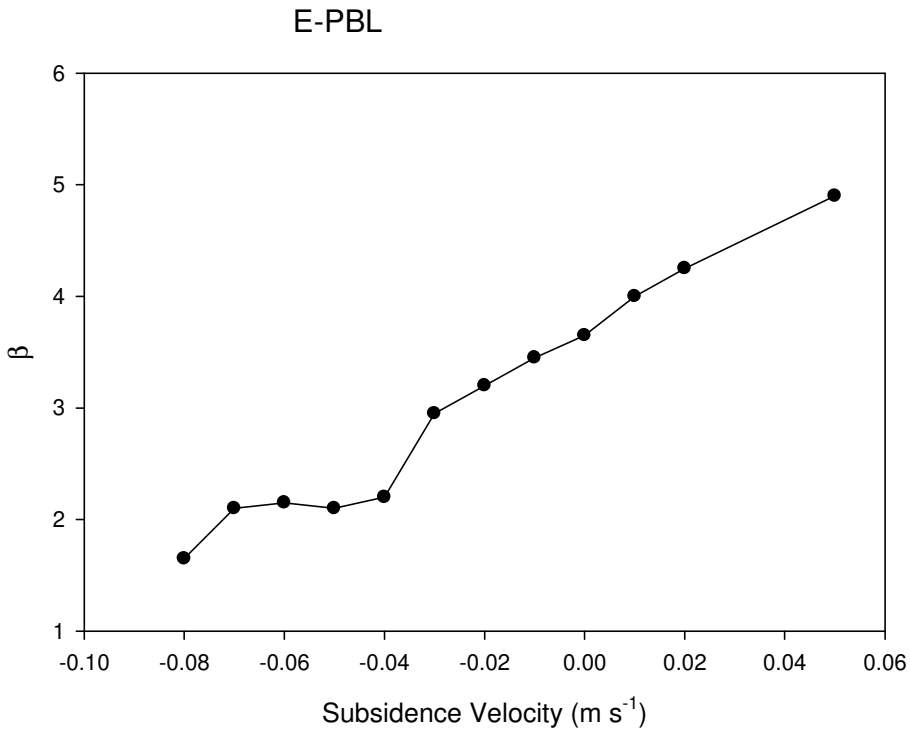

Figure 7 Computations of β using the E-PBL model for a range in subsidence velocities.

Why is β dependent upon subsidence velocity? As can be inferred by Figure 8, conditions that yield a wider range in relative humidity over the course of a day in the planetary boundary layer are associated with lower values of β, and vice versa. With more negative subsidence, boundary layer growth is suppressed, which in turn amplifies the daily range in VPD and air temperature. For example, if the subsidence velocity is -0.05 m s^{-1} peak boundary layer depths range between 1000 and 1400 m. With shallower boundary layers, the diel range in air temperature is between 10 and 15 C and the diel range in vapor pressure deficit is between 1400 and 2000 Pa. Conversely, deeper boundary layers occur with positive subsidence velocities. These conditions dampen the daily range in VPD and air temperature, thereby producing larger β values. For example, if the subsidence velocity is 0.05 m s^{-1} boundary layers as deep as 3000 to 4000 m may form, depending on the surface resistance. In this circumstance the diel range of air temperature is less than 10 C and the diel range in vapor pressure deficit is less than 1100 Pa.

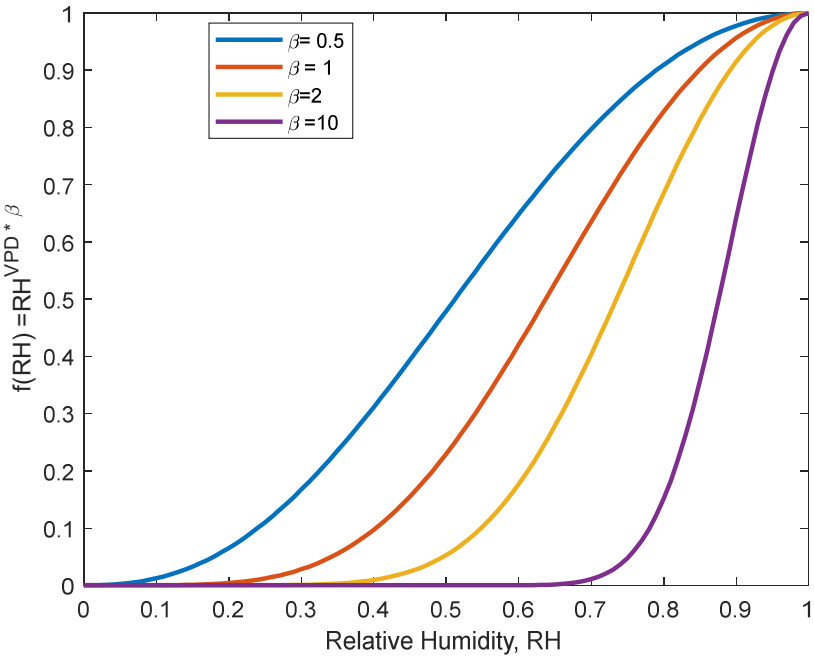

Figure 8 Family of curves demonstrating the shape and dependence of the soil moisture constraint function β. For cases with non-zero values of f(RH), smaller values β are associated with a wider range in relative humidity (RH) increases

A functional dependency of evaporative fraction on soil moisture follows a legacy of prior studies (Chen et al., 2008; Debruin, 1983; Priestley and Taylor, 1972). What is unique here, is the substitution of information on soil moisture with relative humidity. Albeit, the soil moisture stress index has empirical, rather than theoretical origins (Fisher et al., 2008). However, we have shown, based on E-PBL modeling, that it can infer a quantitative measure on the down-regulation of evaporation from vegetated landscapes on monthly time scales.

We confess that our assessment of the soil moisture stress index at the ecosystem scale is tangential to its original application. Traditionally, the soil moisture stress index was applied only to the soil evaporation term of the PT-JPL evaporation model that is the basis of converting ECOSTRESS data into fields of evaporation (Fisher et al., 2020; Fisher et al., 2008). However, based on the interpretation provided by the surface-boundary layer feedbacks, it is plausible that the soil moisture stress index better represents a scale emergent property of total evaporation, the sum of soil evaporation and ecosystem transpiration.

To better visualize how the soil moisture stress index works, we provide a conceptual figure of the feedbacks and linkages between soil moisture, evaporation, humification and growth of the planetary boundary layer for the case of a reduction in soil moisture (Figure 9). On Figure 9 are fast (daily) and slow (seasonal to decadal) loops. On slow, seasonal and climatological time scales a reduction in soil moisture will reduce or limit leaf area index which in turn reduces the net radiation budget that drives latent heat exchange and the amount of leaf surface area from which water transpires. On faster time scales, hours, days and weeks, a reduction in soil moisture has a direct forcing on evaporation by reducing stomatal conductance. This loop reduces evaporation directly. It also mutes the increase of the humidity in the boundary layer by driving the boundary layer to grow deeper and by provide less moisture with which to humidify that boundary layer. A reduction in soil moisture will also reduce the

production of clouds. This loop can increase solar radiation, which increases net radiation and evaporation. Evaporative cooling will reduce surface temperature and this loop can increase net radiation.

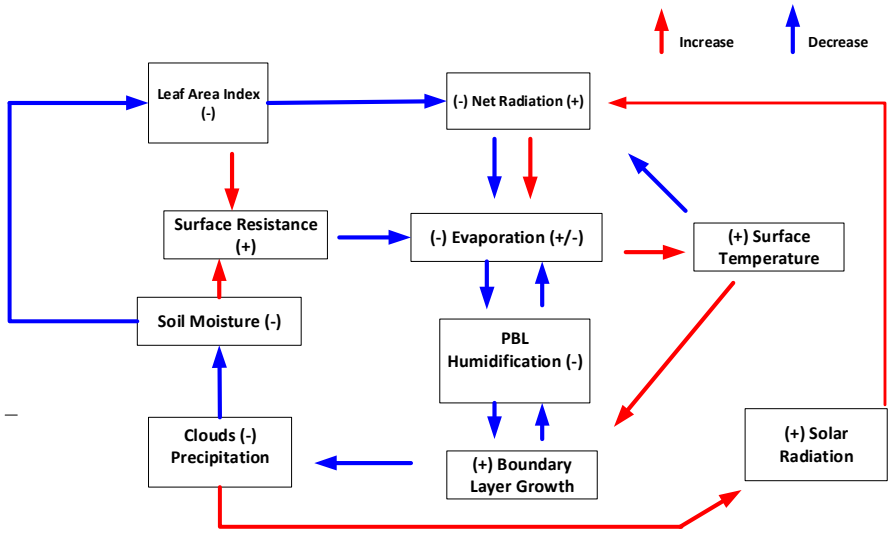

Figure 9 Feedbacks between evaporation, soil moisture, atmospheric humidity and boundary layer growth. Red arrows are associated with a positive forcing and blue arrows are with negative forcing. These result from the change designated by the sign of the process in the box. For example, a reduction in clouds and precipitation will increase solar radiation and decrease soil moisture.

The final question left begging is whether, or not, 'plants act as sensors of soil moisture'? Several global syntheses indicate that on average, transpiration accounts for about 60% of ecosystem evaporation (Schlesinger and Jasechko, 2014; Wei et al., 2017). Based on this evidence some readers may conclude that our claim may be false because so much evaporation comes from soil and rain interception.

While we originally introduced the phase that 'plants act as sensors of soil moisture', as a metaphor we conclude that this phrase has utility as many plants are adept at tapping deeper sources of moisture in the soil and rock that is not routinely measured with soil moisture sensors. And, the extraction of this moisture is evident in how the planetary boundary layer is humidified.

We support this conclusion with the following set of evidence. First, plants have higher areas of evaporating surfaces per meter of ground than soil and plants tap deeper layers of moisture than that associated with soil evaporation. Second, assemblages of plants have the potential to deliver water vapor to the atmosphere at much higher rates that adjacent patches of bare soil. Only when wetted do soils dry quickly, as soil evaporation is a function of the square root of time following a wetting event (Gardner, 1959; Or et al., 2013). And when soil surfaces remain dry, as during long rainless periods over semiarid ecosystems, soil evaporation is tiny during this period. Third, the ratio between transpiration and ecosystem evaporation is conditional on leaf area index (Wei et al., 2017). Soil evaporation will constitute a small fraction of total evaporation under dense canopies with high leaf area indices. In semi-arid and arid landscapes, the relative presence and absence of plants ends up reflecting the status of soil moisture. Consequently, we conclude that the evaporative fraction (the ratio of transpiration to evaporation), per se, is less inclined to alter the humidification of the planetary boundary layer, as compared with the total amount of evaporation, which is strongly controlled by plants.

Future lines of inquiry will require a way to down-regulate evaporation when soil moisture deficits occur on shorter time scales than a month. One possible way involves an empirical connection between surface

conductance and canopy photosynthesis (Dolman et al., 2002; Xu and Baldocchi, 2004). The later variable can be inferred from space with products like reflected near infrared radiation from vegetation (Badgley et al., 2019).

Conclusion

In this analysis, we were able to answer the question, whether information about the state of humidity in the planetary boundary layer can be used to infer how actual evaporation is down-regulated by soil moisture deficits, with an affirmative. This was accomplished using a large and diverse data set of evaporation and meteorological data from the global FLUXNET project. And, by applying these data to parameterize the soil moisture stress index that is used to interpret evaporation from a set of radiation and thermal sensors on the International Space Station by the ECOSTRESS project.

We found that the beta value of soil moisture stress index had a global median value of 1.71, but its value varied across plant functional groups, whose bioclimate ranged from xeric to mesic. Interpreting these results through the lens of a coupled surface energy balance and boundary layer model provided a plausible mechanism to why the index worked, as it scales with surface resistance.

This simple soil moisture stress index may have utility assessing soil moisture deficits in climate, weather and biogeochemical cycling models as it relies on simple inputs such as humidity and temperature. Plus, this approach allows the system to reflect the influence of soil moisture at deeper levels in the soil that may not be detected with satellite remote sensing.

A takeaway point from this study is that plants can serve as vertically-integrated soil moisture sensors through how they help regulate atmospheric humidity deficits, as soil moisture deficits down-regulate evaporative fraction. However, this functional relationship works best at monthly to seasonal time scales, at venues with semi-arid and arid vegetation, as there needs to be enough time to allow an equilibrium to adjust between the conditions of the plants and the planetary boundary layer.

Acknowledgements

This research is supported by the NASA Ecostress program (project 80NSSC20K0166), the DOE Ameriflux Management program, under the Office of Science and the California Agricultural Experiment Station, Stennis McIntyre program.

This work used eddy covariance data acquired and shared by the FLUXNET community, including these networks: AmeriFlux, AfriFlux, AsiaFlux, CarboAfrica, CarboEuropeIP, CarboItaly, CarboMont, ChinaFlux, Fluxnet-Canada, GreenGrass, ICOS, KoFlux, LBA, NECC, OzFlux-TERN, TCOS-Siberia, and USCCC. The FLUXNET eddy covariance data processing and harmonization was carried out by the ICOS Ecosystem Thematic Center, AmeriFlux Management Project and Fluxdata project of FLUXNET, with the support of CDIAC, and the OzFlux, ChinaFlux and AsiaFlux offices.

Reference

Anderson, M. et al., 2019. Impact of Insolation Data Source on Remote Sensing Retrievals of Evapotranspiration over the California Delta. Remote Sensing, 11(3): 216.

Anderson, M.C., Kustas, W.P. and Norman, J.M., 2007. Upscaling Flux Observations from Local to Continental Scales Using Thermal Remote Sensing. Agron. J., 99(1): 240.

Badgley, G., Anderegg, L.D.L., Berry, J.A. and Field, C.B., 2019. Terrestrial Gross Primary Production: Using NIRV to Scale from Site to Globe. Global Change Biology, 0(ja).

Baldocchi, D., 1989. Canopy-atmosphere water vapour exchange: Can we scale from a leaf to a canopy? Estimation of areal evapotranspiration, 177: 21-41.

Baldocchi, D., Ma, S. and Verfaillie, J., 2021. On the inter- and intra-annual variability of ecosystem evapotranspiration and water use efficiency of an oak savanna and annual grassland subjected to booms and busts in rainfall. Global Change Biology, 27(2): 359-375.

Baldocchi, D.D. and Meyers, T., 1998. On using eco-physiological, micrometeorological and biogeochemical theory to evaluate carbon dioxide, water vapor and trace gas fluxes over vegetation: a perspective. Agricultural and Forest Meteorology, 90(1-2): 1-25.

Bastiaanssen, W.G.M., Menenti, M., Feddes, R.A. and Holtslag, A.A.M., 1998. A remote sensing surface energy balance algorithm for land (SEBAL). 1. Formulation. Journal of Hydrology, 212-213: 198-212.

Broyden, C.G., Dennis, J.E., Jr. and More', J.J., 1973. On the Local and Superlinear Convergence of Quasi-Newton Methods. IMA Journal of Applied Mathematics, 12(3): 223-245.

Budyko, M.I., 1974. Climate and Life. Academic Press, New York, NY, 508 pp.

Chen, X., Rubin, Y., Ma, S. and Baldocchi, D., 2008. Observations and stochastic modeling of soil moisture control on evapotranspiration in a Californian oak savanna. Water Resour. Res., 44(8): n/a-n/a.

Cleverly, J. et al., 2013. Dynamics of component carbon fluxes in a semi-arid Acacia woodland, central Australia. Journal of Geophysical Research: Biogeosciences, 118(3): 1168-1185.

D'Odorico, P., Caylor, K., Okin, G.S. and Scanlon, T.M., 2007. On soil moisture–vegetation feedbacks and their possible effects on the dynamics of dryland ecosystems. Journal of Geophysical Research, 112(G4).

Dawson, T.E., Hahm, W.J. and Crutchfield-Peters, K., 2020. Digging deeper: what the critical zone perspective adds to the study of plant ecophysiology. New Phytologist, 226(3): 666-671.

Debruin, H.A.R., 1983. A Model for the Priestley-Taylor Parameter-Alpha. Journal of Climate and Applied Meteorology, 22(4): 572-578.

Dolman, A.J., Moors, E.J. and Elbers, J.A., 2002. The carbon uptake of a mid latitude pine forest growing on sandy soil. Agricultural and Forest Meteorology, 111(3): 157-170.

Entekhabi, D. et al., 2010. The Soil Moisture Active Passive (SMAP) Mission. Proc. IEEE, 98(5): 704-716.

Feddes, R. et al., 2001. Modeling root water uptake in hydrological and climate models. Bulletin of the American Meteorological Society, 82: 2797-2809.

Fisher, J.B. et al., 2020. ECOSTRESS: NASA's Next Generation Mission to Measure Evapotranspiration From the International Space Station. Water Resour. Res., 56(4): e2019WR026058.

Fisher, J.B. et al., 2017. The future of evapotranspiration: Global requirements for ecosystem functioning, carbon and climate feedbacks, agricultural management, and water resources. Water Resour. Res., 53(4): 2618-2626.

Fisher, J.B., Tu, K.P. and Baldocchi, D.D., 2008. Global estimates of the land–atmosphere water flux based on monthly AVHRR and ISLSCP-II data, validated at 16 FLUXNET sites. Remote Sensing of Environment, 112(3): 901-919.

Gardner, W.R., 1959. Solutions of the Flow Equation for the Drying of Soils and Other Porous Media. Soil Science Society of America Journal, 23(3): 183-187.

Grier, C.G. and Running, S.W., 1977. Leaf Area of Mature Northwestern Coniferous Forests: Relation to Site Water Balance. Ecology, 58(4): 893-899.

Hook, S.J., Gabell, A.R., Green, A.A. and Kealy, P.S., 1992. A comparison of techniques for extracting emissivity information from thermal infrared data for geologic studies. Remote Sensing of Environment, 42(2): 123-135.

Jacobs, C.M.J. and Debruin, H.A.R., 1992. The Sensitivity of Regional Transpiration to Land-Surface Characteristics - Significance of Feedback. J. Clim., 5(7): 683-698.

Jarvis, P.G. and McNaughton, K.G., 1986. Stomatal Control of Transpiration: Scaling Up from Leaf to Region. 15: 1-49.

Jiang, C. and Ryu, Y., 2016. Multi-scale evaluation of global gross primary productivity and evapotranspiration products derived from Breathing Earth System Simulator (BESS). Remote Sensing of Environment, 186: 528-547.
Jin, Y., Randerson, J.T. and Goulden, M.L., 2011. Continental-scale net radiation and evapotranspiration estimated using MODIS satellite observations. Remote Sensing of Environment, 115(9): 2302-2319.
Joffre, R. and Rambal, S., 1993. How tree cover influences the water balance of Mediterranean rangelands. Ecology, 74: 570-582.
Jung, M. et al., 2010. Recent decline in the global land evapotranspiration trend due to limited moisture supply. Nature, 467(7318): 951-4.
Jung, M. et al., 2011. Global patterns of land-atmosphere fluxes of carbon dioxide, latent heat, and sensible heat derived from eddy covariance, satellite, and meteorological observations. Journal of Geophysical Research, 116.
Kelliher, F.M., Leuning, R., Raupach, M.R. and Schulze, E.-D., 1995. Maximum conductances for evaporation from global vegetation types. Agricultural and Forest Meteorology, 73(1-2): 1-16.
Kim, J. and Verma, S.B., 1991. Modeling canopy stomatal conductance in a temperate grassland ecosystem. Agricultural and Forest Meteorology, 55(1–2): 149-166.
Konings, A.G., Rao, K. and Steele-Dunne, S.C., 2019. Macro to micro: microwave remote sensing of plant water content for physiology and ecology. New Phytologist, 223(3): 1166-1172.
Koster, R.D. et al., 2004. Regions of Strong Coupling Between Soil Moisture and Precipitation. Science, 305(5687): 1138-1140.
Kustas, W.P. and Daughtry, C.S.T., 1990. Estimation of the soil heat flux/net radiation ratio from spectral data. Agricultural and Forest Meteorology, 49(3): 205-223.
Mallick, K. et al., 2015. Reintroducing radiometric surface temperature into the Penman-Monteith formulation. Water Resour. Res., 51(8): 6214-6243.
Mallick, K. et al., 2013. Latent heat flux and canopy conductance based on Penman–Monteith, Priestley–Taylor Equation, and Bouchet's complementary hypothesis. J. Hydrometeorol., 14(2): 419-442.
McNaughton, K.G. and Jarvis, P.G., 1991. Effects of Spatial Scale on Stomatal Control of Transpiration. Agricultural and Forest Meteorology, 54(2-4): 279-302.
McNaughton, K.G. and Spriggs, T.W., 1986. A Mixed-Layer Model for Regional Evaporation. Boundary-Layer Meteorology, 34(3): 243-262.
Meyer, W.S., Kondrlovà, E. and Koerber, G.R., 2015. Evaporation of perennial semi-arid woodland in southeastern Australia is adapted for irregular but common dry periods. Hydrol. Process., 29(17): 3714-3726.
Miller, G.R., Chen, X., Rubin, Y., Ma, S. and Baldocchi, D.D., 2010. Groundwater uptake by woody vegetation in a semiarid oak savanna. Water Resour. Res., 46(10): n/a-n/a.
Miralles, D.G., De Jeu, R.A.M., Gash, J.H., Holmes, T.R.H. and Dolman, A.J., 2011. Magnitude and variability of land evaporation and its components at the global scale. Hydrology and Earth System Sciences, 15(3): 967-981.
Molod, A., Salmun, H. and Waugh, D.W., 2003. A New Look at Modeling Surface Heterogeneity: Extending Its Influence in the Vertical. J. Hydrometeorol., 4: 810-825.
Monteith, J.L., 1965. Evaporation and Environment, Symposium Society of Experimental Biology XIX, pp. 205-234.
Monteith, J.L., 1981. Evaporation and Surface-Temperature. Q. J. R. Meteorol. Soc., 107(451): 1-27.
Mu, Q., Heinsch, F.A., Zhao, M. and Running, S.W., 2007. Development of a global evapotranspiration algorithm based on MODIS and global meteorology data. Remote Sensing of Environment, 111(4): 519-536.

Mu, Q., Zhao, M. and Running, S.W., 2011. Improvements to a MODIS global terrestrial evapotranspiration algorithm. Remote Sensing of Environment, 115(8): 1781-1800.
Myrup, L.O., Morgan, D.L. and Boomer, R.L., 1983. Summertime Three-Dimensional Wind Field Above Sacramento, California. Journal of Climate and Applied Meteorology, 22(2): 256-265.
Novick, K.A. et al., 2016. The increasing importance of atmospheric demand for ecosystem water and carbon fluxes. Nat. Clim. Chang., 6(11): 1023-1027.
Or, D., Lehmann, P., Shahraeeni, E. and Shokri, N., 2013. Advances in soil evaporation physics—A review. Vadose Zone J., 12(4): vzj2012. 0163.
Papale, D. et al., 2012. Database Maintenance, Data Sharing Policy, Collaboration. In: M. Aubinet (Editor), Eddy Covariance: A Practical Guide to Measurement and Data Analysis. Springer.
Pastorello, G. et al., 2020. The FLUXNET2015 dataset and the ONEFlux processing pipeline for eddy covariance data. Scientific Data, 7(1): 225.
Paw U, K.T. and Gao, W., 1988. Applications of solutions to non-linear energy budget equations. Agricultural and Forest Meteorology, 43: 121-145.
Priestley, C.H.B. and Taylor, R.J., 1972. On the assessment of surface heat flux and evaporation using large-scale parameters. Monthly Weather Review, 100: 81-92.
Purdy, A.J. et al., 2018. SMAP soil moisture improves global evapotranspiration. Remote Sensing of Environment, 219: 1-14.
Purdy, A.J., Fisher, J.B., Goulden, M.L. and Famiglietti, J.S., 2016. Ground heat flux: An analytical review of 6 models evaluated at 88 sites and globally. Journal of Geophysical Research: Biogeosciences, 121(12): 3045-3059.
Rambal, S., 1984. Water balance and pattern of root water uptake by a Quercus coccifera L. evergreen scrub. Oecologia, 62: 18-25.
Raupach, M.R., 1991. Vegetation-Atmosphere Interaction in Homogeneous and Heterogeneous Terrain - Some Implications of Mixed-Layer Dynamics. Vegetatio, 91(1-2): 105-120.
Raupach, M.R., 1995. Vegetation-atmosphere interaction and surface conductance at leaf, canopy and regional scales. Agricultural and Forest Meteorology, 73(3-4): 151-179.
Raupach, M.R., 2000. Equilibrium evaporation and the convective boundary layer. Boundary-Layer Meteorology, 96(1-2): 107-141.
Rebmann, C. et al., 2018. ICOS eddy covariance flux-station site setup: a review. International Agrophysics, 32(4): 471-+.
Rey-Sanchez, C. et al., 2021. Evaluation of Atmospheric Boundary Layer Height From Wind Profiling Radar and Slab Models and Its Responses to Seasonality of Land Cover, Subsidence, and Advection. Journal of Geophysical Research: Atmospheres, 126(7): e2020JD033775.
Rigden, A.J. and Salvucci, G.D., 2015. Evapotranspiration based on equilibrated relative humidity (ETRHEQ): Evaluation over the continental US. Water Resour. Res., 51(4): 2951-2973.
Rodriguez-Iturbe, I., 2000. Ecohydrology: A hydrologic perspective of climate-soil-vegetation dynamics. Water Resour. Res., 36(1): 3-9.
Sabbatini, S. et al., 2018. Eddy covariance raw data processing for CO2 and energy fluxes calculation at ICOS ecosystem stations. International Agrophysics, 32(4): 495-+.
Salvucci, G.D. and Gentine, P., 2013. Emergent relation between surface vapor conductance and relative humidity profiles yields evaporation rates from weather data. Proc. Natl. Acad. Sci. U. S. A., 110(16): 6287-91.
Sankaran, M. et al., 2005. Determinants of woody cover in African savannas. Nature, 438(7069): 846-9.
Schlesinger, W.H. and Jasechko, S., 2014. Transpiration in the global water cycle. Agricultural and Forest Meteorology, 189-190: 115-117.
Schulze, E.-D. and Hall, A., 1982. Stomatal responses, water loss and CO 2 assimilation rates of plants in contrasting environments, Physiological plant ecology II. Springer, pp. 181-230.

Schulze, E.D., Leuning, R. and Kelliher, F.M., 1995. Environmental regulation of surface conductance for evaporation from vegetation. Vegetatio, 121(1-2): 79-87.
Seneviratne, S.I. et al., 2010. Investigating soil moisture–climate interactions in a changing climate: A review. Earth-Science Reviews, 99(3-4): 125-161.
Siqueira, M., Katul, G. and Porporato, A., 2009. Soil Moisture Feedbacks on Convection Triggers: The Role of Soil–Plant Hydrodynamics. J. Hydrometeorol., 10(1): 96-112.
Sperry, J.S., 2000. Hydraulic constraints on plant gas exchange. Agricultural and Forest Meteorology, 104(1): 13-23.
Stewart, J.B. and Verma, S.B., 1992. Comparison of Surface Fluxes and Conductances at Two Contrasting Sites Within the FIFE Area. J. Geophys. Res., 97(D17): 18623-18628.
Stoy, P.C. et al., 2019. Reviews and syntheses: Turning the challenges of partitioning ecosystem evaporation and transpiration into opportunities. Biogeosciences Discuss., 2019: 1-47.
van Heerwaarden, C.C., Vilà-Guerau de Arellano, J., Moene, A.F. and Holtslag, A.A.M., 2009. Interactions between dry-air entrainment, surface evaporation and convective boundary-layer development. Q. J. R. Meteorol. Soc., 135(642): 1277-1291.
Verma, M. et al., 2016. Global Surface Net-Radiation at 5 km from MODIS Terra. Remote Sensing, 8(9): 739.
Wallace, J.M. and Hobbs, P.V., 1977. Atmospheric Science, An Introductory Survey. Academic Press, San Diego, CA, 465 pp.
Wei, Z. et al., 2017. Revisiting the contribution of transpiration to global terrestrial evapotranspiration. Geophys. Res. Lett., 44(6): 2792-2801.
Wolf, S. et al., 2016. Warm spring reduced carbon cycle impact of the 2012 US summer drought. Proceedings of the National Academy of Sciences.
Xu, L. and Baldocchi, D.D., 2003. Seasonal trend of photosynthetic parameters and stomatal conductance of blue oak (Quercus douglasii) under prolonged summer drought and high temperature. Tree Physiol., 23: 865-877.
Xu, L. and Baldocchi, D.D., 2004. Seasonal variation in carbon dioxide exchange over a Mediterranean annual grassland in California. Agricultural and Forest Meteorology, 123(1-2): 79-96.